A spatiotemporal map of the aging mouse brain reveals white matter tracts as vulnerable foci

Authors: Oliver Hahn[1,2], Aulden G Foltz[1,2], Micaiah Atkins[1,2†], Blen Kedir[1,2†], Patricia Moran-Losada[1,2], Ian H Guldner[1,2], Christy Munson[1,2,3], Fabian Kern[4,5], Róbert Pálovics[1,2], Nannan Lu[1,2], Achint Kaur[1,2], Jacob Hull[1,2], John R Huguenard[1,2], Andreas Keller[4,5], Benoit Lehallier[6], Tony Wyss-Coray[1,2,7,8]*

Affiliations:

[1]Department of Neurology and Neurological Sciences, Stanford University School of Medicine, Stanford, California, USA.

[2]Wu Tsai Neurosciences Institute, Stanford University School of Medicine, Stanford, California, USA

[3]Vilcek Institute of Graduate Biomedical Sciences, NYU Langone Health, New York City, New York, USA

[4]Clinical Bioinformatics, Saarland University, Saarbrücken, Germany

[5]Helmholtz-Institute for Pharmaceutical Research Saarland (HIPS), Helmholtz-Centre for Infection Research (HZI), Saarbrücken, Germany

[6]Alkahest Inc., San Carlos, CA

[7]Paul F. Glenn Center for the Biology of Aging, Stanford University, Stanford, California, USA

[8]Stanford University, The Knight Initiative for Brain Resilience, Stanford, California, USA

* Corresponding author. Email: twc@stanford.edu

† These authors contributed equally to this work: Micaiah Atkins, Blen Kedir.

Abstract: Aging is the key risk factor for loss of cognitive function and neurodegeneration but our knowledge of molecular dynamics across the aging brain is very limited. Here we perform spatiotemporal RNA-seq of mouse brain aging, encompassing 847 samples from 15 regions spanning 7 ages. We identify a brain-wide gene signature representing aging in glia with spatially-defined magnitudes. By integrating spatial and single-nuclei transcriptomics, we reveal that glia aging is profoundly accelerated in white matter compared to cortical areas. We further discover region-specific expression changes in specialized neuronal populations. Finally, we discover distinct clusters of brain regions that differentially express genes associated with 3 human neurodegenerative diseases, highlighting regional aging as a potential modulator of disease. Our findings identify molecular foci of brain aging, providing a foundation to target age-related cognitive decline.

One-Sentence Summary: Cartography of gene expression changes across the central nervous system of mice identifies hotspots of accelerated brain aging.

Main Text: Aging is the predominant risk factor for cognitive dysfunction (*1*, *2*) and several neurodegenerative disorders, including Alzheimer's disease (AD) and Parkinson's disease (PD) (*3–5*). It remains unclear though, how aging contributes to the development of these distinct diseases of the brain, given their differences in pathological hallmarks, time of onset, and, notably, the regions affected (*4*). A quantitative understanding of the dynamics of aging across the brain may provide new insight into the relationship between aging and neurodegeneration. Interestingly, neuroimaging studies using structural and functional magnetic resonance imaging (MRI) data indicate that aging impacts the brain in a region-specific manner (*6*, *7*). However, these structural manifestations provide limited insight into the underlying molecular alterations occurring during brain aging. In contrast, changes in gene expression can be a readout of cellular deterioration and molecular processes accompanying aging, permitting quantitative comparisons of aging rates between tissues (*8*) and cell types (*9*). Previous studies have profiled age-related gene expression changes in human brain tissue, yet these microarray-based experiments capture a limited set of transcripts and cover usually one to four regions (*10*, *11*) or quantify the transcriptome at low temporal resolution (*12*, *13*). Expression profiling during human brain aging is particularly challenging since it can take hours to days before postmortem tissue is stabilized (*13–15*). Alternatively, expression profiling in model organisms like *M. musculus* enables quantitative data with minimal confounding factors, but comprehensive studies covering more than a few regions and at high temporal resolution (*16–19*) do - to our knowledge - not exist.

Results

Spatiotemporal quantification of age-related gene expression across the mouse brain

To obtain a deep molecular understanding of the spatiotemporal changes of the aging mammalian brain, we selected 15 brain regions in the mouse with critical functions in cognition,

whole-body metabolic control, or human disease. We punched out brain regions from coronal brain sections from the left and right hemisphere, including three cortical regions (motor area, visual area and entorhinal cortex; Mot.cor., Vis.cor and Ent.cor, respectively), anterior (dorsal) and posterior (ventral) hippocampus (Hipp.ant and Hipp.post., respectively), hypothalamus (Hypoth.), thalamus, caudate putamen (part of the striatum; Caud.put.), pons, medulla, cerebellum (Cereb.) and the olfactory bulb (Olf.bulb). We further isolated three regions that were enriched with the corpus callosum (Corp.cal.), choroid plexus (Chor.plx.) and the neurogenic subventricular zone (SVZ), (Fig. S1A). We then applied our method to 59 mice (Fig. 1A; n = 3-6 males per age; aged 3, 12, 15, 18, 21, 26 and 28 months; n = 5 females per age; aged 3, 12, 15, 18 and 21 months; all C57BL/6JN strain), resulting in a total of 1,770 samples (885 samples from each hemisphere). Isolated regions from the left hemisphere were stored, while all right hemisphere regions were processed through a custom-built bulk RNA-seq (bulk-seq) pipeline (Fig. 1B, Methods). We achieved robust tissue sampling with high RNA quality while minimizing perfusion artifacts, as indicated by consistent RNA yields across samples from the same region (Fig. S1B), median RNA integrity numbers of 9.45 out of 10 (Fig. S1C) (*20*), and a neglectable fraction of reads mapping to hemoglobin genes (Fig. S1D). In comparison, the UK Brain Expression Consortium, one of the largest collections of human brain tissue, reports average RNA integrity numbers of 3.85 for their tissue samples (*13*, *14*).

After quality control, we obtained 847 single-region transcriptomes. Visualization in uniform manifold approximation and projection (UMAP) space separated samples by region (Fig. 1C), but not sex or age, which concurred with deterministic shared-nearest-neighbors graph clustering and hierarchical clustering (Fig. S2A-E). However, within individual regions, samples segregated transcriptionally by age. The comparatively subtle effect of aging on gene expression

highlights the necessity for precise isolation of brain tissue to avoid confounding cross-region contamination (Fig. 1D and S2A).

To assess if the isolated regions accurately captured a given brain structure's transcriptome, we analyzed the expression of region-enriched genes ('marker genes'; Methods and data S1) in a publicly-available spatial transcriptomics dataset of an adult male mouse brain (*21*). To this end, we combined marker genes of a given region into 'signatures' (*22*) that represent its transcriptional fingerprint. For each signature, we calculated a score per spatial transcriptome spot, summarizing the expression of marker genes into a single value. Signature scores were distinctly elevated in areas corresponding to the anatomical structures annotated in the Allen brain reference atlas (Fig. S3A) (*23*). Notably, the corpus callosum-derived signature demarcated fiber tracts throughout the brain, indicating that the sampled transcriptome of this region could be a proxy for white matter tracts in general (Fig. S3A). To assess the isolation of the SVZ, we built a signature of activated neural stem cells (aNSC) based on marker genes from single-cell data (*24*) and calculated the score per each region. These aNSCs are enriched in neurogenic areas at young age and their number declines in old individuals (*24*). Not only was the score elevated in the aNSC-rich olfactory bulb and SVZ region but we also found a significant decline with age, thus capturing the loss of neurogenesis, a known phenomenon of mouse brain aging (Fig. S3B) (*24*). In summary, our tissue isolation and bulk-seq workflow yielded high-quality transcriptomes that robustly captured a region's gene expression profile across a cohort of mice. The data can be interactively explored at https://twc-stanford.shinyapps.io/spatiotemporal_brain_map/.

Region identity is linked to expression dynamics during aging

RNA-seq permits quantitative comparisons of aging rates between organs and cell types (*8*, *19*) based on timing and effect size of gene expression shifts. For instance, we found substantial

region-dependence in the magnitude and timing of *C4b* expression (Fig. 1E), a complement component and major schizophrenia risk factor (*25*) that is robustly up-regulated in aged mice (*26*) and models of neurodegeneration (*27*). Notably, recent single-cell studies revealed that the composition of major cell types remains almost constant throughout the aging mouse brain (*28*), thus the expression dynamics observed in bulk are unlikely to be driven primarily by shifts in cell type abundance. Thus, we were able to use our temporally resolved data to probe the per-region impact of aging on gene expression over time, as this could help to identify structures with selective vulnerability to old age.

We performed pairwise differential expression between 3 months and every following age group to determine when differentially expressed genes arise (DEGs; used from hereon to refer to genes that change with age). To focus on high-confidence expression changes that persist with advancing age, a gene had to pass the statistical cutoff in at least two comparisons to be classified as a DEG (Fig. 1E-G). The general trend across regions indicated an increase of DEGs over time that plateaued around 21 months (Fig. 1F,G), yet individual regions varied profoundly with respect to their total number of DEGs and the trajectory of DEG accumulation (Fig. 1F and data S2). For instance, the visual cortex showed a steady increase of DEGs until late age, while the transcriptome of the motor cortex already exhibited significant perturbation at 12 months, but there was little increase until a sudden jump at 21 months (Fig. 1F,G). In contrast, the transcriptome of the entorhinal cortex appeared largely refractory to the effects of age altogether, with only 13 detectable DEGs in total (Fig. 1F,G). This is in line with human MRI (*7*) and microarray (*29*) studies demonstrating that the entorhinal cortex displays only mild alterations during cognitively normal human aging, whereas it frequently exhibits the first amyloid deposition in AD patients (*30*). Together, these results reveal that the effect size of expression shifts during brain aging are strikingly region- and time-dependent, highlighting the necessity for region-resolved

quantification and analysis. Notably, the regions with the most profound and earliest shifts in gene expression were the white matter-rich caudate putamen, cerebellum and corpus callosum, the latter showing a tenfold increase in the number of DEGs between 12 and 18 months.

Since pairwise comparisons treat every gene and age group independently, we next validated these results with two independent analyses. First, we probed all genes in the genome for positive or negative correlation with age (Spearman's rho ≥ 0.5 or ≤ -0.5, respectively; padj ≤ 0.05; data S3), thus taking all age groups into account (Fig. 1H). Not only did the regions differ in the number of age-correlated genes, confirming that the effect size of age depends on the region, but also the corpus callosum and cerebellum were the most impacted, while the entorhinal cortex remained largely unaffected (Fig. 1H). As a second validation, we performed weighted gene co-expression network analysis (WGCNA) (*31*) for each region (Methods; data S4), clustering genes into modules which might be driven by similar regulation during aging. We filtered for modules exhibiting significant association with age and found the number of modules differed between regions. In line with the above results, we found seven or more modules in the corpus callosum, cerebellum and motor cortex, whereas we detected no age-related modules in the entorhinal cortex (data S4). To gain biological insight, we performed cell type- and pathway-enrichment for each age-related module and compiled summarized reports for each region as a quick reference resource for the scientific community (https://twc-stanford.shinyapps.io/spatiotemporal_brain_map/). Interestingly, we discovered in 10 regions at least one module with increased expression over time that was enriched for microglia- and inflammation-related genes (Fig 1I,J). Consistent with these findings, we found a small, common set of differentially regulated genes, including neuroinflammatory markers *Fcgr2b*, *Ctss*, *Cst7* (*32*) in modules across regions, suggesting the presence of a minimal group of co-regulated genes changing throughout the brain. In summary, we found the results of three independent analyses (pairwise tests, age-correlation and WGCNA)

congruent, demonstrating that the observed effects of aging on the transcriptome are region specific.

A minimal gene set forms a common fingerprint of brain aging

WGCNA analysis results indicated the possibility of a shared gene set that changes during aging throughout the brain. Such a minimal age-related gene signature would permit quantitative comparisons of the rates of change in a region's transcriptional age. While the vast majority of DEGs appeared to change only in three or less regions, indicative of region-selective expression patterns, we found 82 genes that were differentially regulated in 10 or more regions (Fig. 2A,B; data S2). These were strongly enriched for up-regulated genes with immune-modulatory functions (data S5), including MHC I-mediated antigen presentation, interferon-response, cell adhesion and complement cascade, as well as regulators of mouse microglia activity (Fig. 2C) including *Cd22* (*33*), *Trem2* and *Tyrobp* (*34*). Interestingly, of the only 7 down-regulated genes in this set, we found protein homeostasis genes *Dnajb1*, *Hsph1* and *Ahsa1*, as well as collagen synthesis gene *P4ha1*, which is in line with perturbed protein quality control mechanisms as a hallmark of aging (*3*) (Fig. 2B). We combined these 82 genes into a common RNA aging signature to calculate their expression as a single 'common aging score' (CAS; Methods) for each mouse and region. While the CAS expectedly showed significant increases in every region (Fig. 2D, Fig. S4A), the shape and amplitude of the trajectories varied profoundly. The pace and direction with which the CAS changed with age is defined from here on as a region's 'CAS velocity'. We employed linear models to approximate these trajectories, using the slope of the linear fit as a metric to comparatively assess the CAS velocity across regions (Fig. 2D,E). Of note, the CAS at baseline (i.e. the offset of the linear fit) did not predict a region's CAS velocity (Fig. 2F). Our analysis revealed a gradient of velocities across regions, with the three cortical areas and the olfactory bulb ranking last, at

approximately one-third of the velocity of the corpus callosum, the 'fastest' region (Fig. 2G). Other white matter-rich areas such as the caudate putamen also exhibited high velocities, while the hippocampus, thalamus and hypothalamus - some of the most investigated regions in mouse and human brain aging research (*18*) - ranked slightly below average. The median CAS across all regions associated with the animals' chronological age (Fig. S4B). Yet, the regions' differing velocities resulted in increased per-animal variance, indicating that the transcriptional state of this gene set becomes profoundly desynchronized across the brain. This appeared to be independent of the regions' anatomical location, as the fast-aging corpus callosum stretches between the slow-aging cortical areas and hippocampus (Fig. 2H). Interestingly, when we examined the CAS trajectories for the interval between 3 and 21 months, we observed moderate but significant acceleration of the CAS in females compared to males (Fig. 2I, S4C,D). In particular, the hypothalamus exhibited the most pronounced acceleration in females (Fig. S4D), with the thalamus and corpus callosum indicating a similar trend. These findings are in line with human studies reporting more pronounced expression of immune-related genes in the hippocampus and cortex of aged women (*29*, *35*). Our data could advance the understanding of several sexual-dimorphisms observed in the brain, including the higher age-specific risk of dementia among women (*36*) in general, and the dynamics of reproductive aging in particular, given the hypothalamus' critical role in regulating reproduction, development and metabolism (*37*).

Fiber tracts are foci of accelerated brain aging

Bulk-seq data - even with the regional dissection conducted here - could mask transcriptional changes with age that occur in sub-structures of regions, such as specific layers of the cortex. We thus aimed to validate our CAS analysis with a fine-resolution method that would still capture multiple regions in the same assay. To this end, we performed spatial transcriptomics

(Spatial-seq) of the brain across aging, isolating coronal sections from an independent cohort of male mice aged 6, 18, and 21 months (Fig. 2J). Using a clustering-based approach to annotate the regional identity of Spatial-seq spots (Fig. S5A,B; Methods; data S6) we identified them as belonging to the hippocampus, cortex (motor and somatosensory area), thalamus, hypothalamus, striatum (including the caudate putamen), choroid plexus and white matter fiber tracts (including the corpus callosum) (Fig. 2K and S5C-F). Our data demonstrated robust capture of the same regions across age groups and individuals (Fig. S5G-L), thus enabling the comparison of DEGs found in bulk-seq with spatial-seq data (data S7). We confirmed a more pronounced regulation of DEGs in the white matter cluster (equivalent to the dissected corpus callosum region) compared to the cortex cluster (equivalent to the motor cortex region), including several of the 82 CAS genes (Fig. 2L, data S7) such as *Trem2* (Fig. 2M). Calculating CAS for each Spatial-seq spot identified a distinct, spatially-confined increase of the score along the white matter tracts, including not only the corpus callosum but also other fiber tract sub-structures such as the fimbria and internal capsule (Fig. 2N,O). In the cortex, however, we observed only a mild increase of CAS with age. In general, CAS velocities calculated via bulk-seq and those calculated via spatial-seq data were well-correlated (Fig. 2P), confirming vastly differing aging velocities between proximal regions *in-situ*.

Heterogeneous velocity of CAS is encoded by glial transcripts

We next sought to quantify the activity of the CAS genes at the single-cell level to identify the cell type(s) that shape the heterogeneous expression dynamics across brain regions. We chose the anterior hippocampus as a representative region given its intermediate CAS velocity (Fig. 2G), utilizing frozen punches from the left hemispheres of the bulk-seq cohort (Fig. 3A). Single-nuclei sequencing (nuc-seq) yielded all major cell types, with no evidence for a shift in cell type composition with age or sex. We observed the highest baseline CAS in microglia, in line with

several of the CAS genes being known immune-response genes (Fig. 2B,C). While the CAS showed a statistically significant increase in all cell types (Fig. 3B), including a mild elevation in several neuronal populations, the most accentuated increase was observed in microglia (Fig. 3C), followed by mature oligodendrocytes, brain endothelial cells (BECs), astrocytes and oligodendrocyte progenitor cells (OPCs). Upon closer examination of the 82 genes, it became clear how the CAS could reflect aging dynamics for several cell types beyond microglia by cell type-specific or cell type-selective gene expression shifts (Fig. 3D), including *Gfap* (Astrocytes; Fig. S6A), *C4b* (Astrocytes and mature oligodendrocytes; Fig. S6B-E), *Gpr17* (OPCs; Fig. S7A-E) and *H2-Q7* (BECs; Fig. S7F). Of note, this analysis also demonstrated that aging can induce expression of genes that are not detected at young age. For instance, *C4b* was mostly expressed in astrocytes at young age, however its expression became detectable and increased foremost with age in mature oligodendrocytes (Fig. S6E). Similarly, expression of *H2-Q7* only became detectable in BECs with old age (Fig. S7F). We validated our findings in an independent dataset, using publicly available scRNA-seq data from dissected SVZ of young and old male mice (*24*) (Fig. S8A). Though generated using a different cohort, region and method, the CAS increase was most pronounced in microglia which is consistent with our data (Fig. S8B-G). There was also a profound increase of CAS in aNSCs, though the very low number of cells at 28 months (less than 50 per animal) complicates robust calculations of CAS at this age. Thus, the region-to-region differences in CAS velocity are predominantly reflecting age effects in non-neuronal cell types, with microglia having the strongest contribution.

Transcriptional aging of microglia is region-dependent

We finally examined if there were varying CAS dynamics between microglia from regions with fast or slow CAS velocity. To this end, we analyzed scRNA-seq data from the *Tabula Muris*

consortium (Fig. 4A), where comparable numbers of microglia were collected from the freshly-isolated cerebellum, striatum, hippocampus and cortex, which we considered sufficient equivalents to the cerebellum, caudate putamen (both areas with high velocity), anterior hippocampus (medium velocity) and motor/visual cortex (low velocity) regions (compare Fig. 2G). Indeed, as predicted by our bulk-seq results, the CAS in aged microglia increased in all four regions significantly, though with greater magnitude in the cerebellum and striatum, followed by the hippocampus and cortex, respectively (Fig. 4B). The same trend was detectable on the level of individual CAS genes, like *Trem2* (Fig. 4C). Notably, there was no detectable CAS difference among microglia at young age across the striatum, hippocampus and cortex, while the cerebellum-derived microglia exhibited a slightly higher CAS at baseline. We conclude that the CAS velocities observed in bulk- and spatial-seq data are, in part, representing microglia that exhibit region-specific magnitudes of aging. Future studies should examine if other non-neuronal cells, like mature oligodendrocytes or BECs, would exhibit a similar CAS heterogeneity.

Neuronal transcripts encode region-specific expression patterns

Given that the CAS genes represent only 1.5% of all DEGs (Fig. 2A; data S2), we hypothesized that the remainder could represent region-specific expression shifts. We first compared age-related DEGs across mouse organs to construct organ-specific signatures of aging (Fig. S9, Methods). The presence of gene sets with specific regulation found in functionally distinct organs led us to investigate whether individual brain regions exhibit a similar degree of specificity during aging. We found that the number of region-specific DEGs varies greatly (Fig. 5A), which we utilized to build aging signatures for each region before calculating the respective score across all other regions (Fig. 5B,C, Fig. S10A,B). As exemplified by the specific signature of the caudate putamen - a region marked by intertwined gray and white matter structures - we

found that most region-specific scores increased with age predominantly in the region on which they were based (Fig. 5B-D and Fig. S10A,B). Except for the thalamus, pons and SVZ, a given region's signature velocity outperformed those of all other regions. Thus, dozens to hundreds of genes in the brain are regulated in a region-specific or -selective manner, revealing highly compartmentalized effects of aging within a single organ.

Notably, signature genes appeared to be functionally connected, as exemplified by the caudate putamen-specific signature which was enriched for down-regulated mitochondrial processes and up-regulated cell adhesion and lipid binding functions (Fig. 5E and data S8). To map out the cell types driving this region-specific signature, we analyzed nuc-seq data from the left hemisphere punches of the anterior hippocampus (Fig. 3A) and caudate putamen (Fig. 4F), where we captured non-neuronal cell types as well as striatum-specific D1- and D2-type medium spiny neurons (D1 and D2 MSNs, respectively). We were able to map several signature genes like *Fgf16*, *S100a10* and *Fabp4* (Fig. S10C-E) to distinct cell populations (Fig. 5G, Methods and data S9) suggesting that bulk tissue can indeed capture the expression dynamics of specific cell subsets. Similar to the cell-resolved analysis of the CAS (Fig. 3B), we calculated several region-specific signature scores for each cell type in young and old individuals. We found a distinct increase of the caudate putamen-specific signature in D1 and D2 MSNs which was not seen with signatures from other regions (Fig. 5H). For instance, expression of muscarinic acetylcholine receptor gene *Chrm3* dropped significantly in the caudate putamen, reflecting down-regulation of this gene specifically in D2 MSNs (Fig. 5I,J). In comparison, dentate gyrus granule cells of the hippocampus exhibited a distinct increase of the hippocampus-specific signature (Fig. 5K), and we found granule cell-specific regulation of several signature genes such as axon-guidance receptor *Unc5d* (*38*) as well as transcription factor *Onecut1* (Fig. 5L,M, Fig. S11A,B). Interestingly, *Onecut2*, a member of the same transcription factor family, exhibited selective regulation in the corpus callosum and

caudate putamen, namely D1 and D2 MSNs (Fig. S11C,D). Onecut transcription factors have only been recently investigated in the CNS as regulators of neuronal differentiation and their motif is a hotspot of DNA single-strand break repair in neurons (*39*). This may indicate that the transcriptome of neuronal populations could be regulated selectively through age-related activity of specific transcription factors.

Finally, we explored whether the biological processes associated with signature genes could indicate differential transcriptional activity across whole pathways or organelles. We observed a significant down-regulation of several mitochondria-related genes in the caudate putamen, including several members of the electron transport chain, which could be indicative of impaired mitochondrial function (Fig. 5E). We identified in this region a global, gradual down-regulation of all genes coding for mitochondria-related proteins (Fig. S11E), as well as a significant drop in scores for a corresponding mitochondrial signature in aged D2 MSNs, mature oligodendrocytes, and astrocytes (Fig. S11F). This was not detected in cell types from the hippocampus or the SVZ (Fig. S11F). This specific down-regulation of mitochondrial processes in aged striatum could help to explain previous observations demonstrating selective vulnerability to mitochondrial toxins and stresses in the striatum of old animals (*40*, *41*).

In conclusion, we discovered extensive region-specific transcriptional signatures of aging that are largely encoded by expression shifts in distinct neuronal subpopulations reflective of a region's specialization.

Aging results in region-specific expression changes of genes associated with human diseases

Genome-wide association studies (GWAS) can identify candidate genes whose genetic makeup impacts the risk of developing a given disease. We thus wondered if mouse homologues of human GWAS genes implicated in neurodegenerative disorders would be differentially

regulated in specific regions during aging. We assembled lists of GWAS genes for AD, PD and multiple sclerosis (MS) (*42*, *43*), and asked if they were significantly enriched among age-related DEGs of a given region (data S10). We further clustered regions that share differentially expressed disease-associated genes, allowing us to find anatomical 'hubs'. Interestingly, each of the three disease-associated gene sets exhibited a different enrichment pattern (Fig. 6A-C) and a varying number of associated genes (Fig. 6D-F). MS genes, for instance, showed significant associations with DEGs from nine different regions that fell into two clusters, indicating two disparate subsets. One cluster consisted of several regions, including the corpus callosum and cerebellum, that up-regulated a shared set of inflammation-related genes such as *Stat3*, *Ly86* and *Irf8*, all of which were also part of the CAS (Fig. 6A). This raises the intriguing possibility of similarities between the pathophysiology of inflammation and demyelination associated with MS and the accelerated aging observed in white matter-rich areas. The visual and motor cortex regions formed the second cluster, exhibiting even numbers of up- and down-regulated MS genes. This supports recent evidence indicating transcriptional shifts (e.g. of *Cbln2*, Fig. 6G) in cortical areas that can occur far away from the actual lesions (*44*) and highlights the need to broadly study regional patterns of gene expression to understand the role of MS-associated genes.

GWAS hits for AD included genes that are currently under intense mechanistic investigation, including *Apoe*, *Ms4a6d*, *Plcg2* and *Gab2* (*45*) (Fig. 6B,H). They were part of DEGs that are upregulated in a small cluster of three regions: the choroid plexus, corpus callosum, and pons, suggesting a different region-specific regulation of these genes as a potential modulator of disease presentation. In contrast, PD-related genes, like the neuroprotective gene *Ip6k2 (46)* (Fig. 6I), were not concentrated within a cluster of regions but rather distributed across the choroid plexus, cerebellum, SVZ, and visual cortex with limited overlap (Fig. 6C). This pattern indicates a disperse regulation of disease-associated genes among the regions studied, which can add to our

understanding of how and where PD may progress. Of note, the substantia nigra, a major region where PD typically manifests, was not quantified in our study.

Taken together, our data demonstrate that genetic risk factors linked to three major neurological and neurodegenerative diseases are affected by age in a region-selective manner. While we cannot predict whether the directionality of the regulation itself has a biological consequence, we consider that the region-specific differential regulation of such genes could be an additional factor modulating disease risk.

Discussion

We report here a comprehensive spatiotemporal map of gene expression across the mouse brain throughout the adult lifespan, consisting of 847 bulk, 16,277 spatial spot and 81,616 single-cell transcriptomes - supported by several publicly available spatial- and scRNA-seq datasets. We find that aging affects regional transcriptomes with widely varying magnitude and timing, including the expression of risk genes for neurodegenerative disorders. Gene expression shifts during aging fall into two general categories: a single set of 82 genes that reflects shared aging dynamics of glia cells with spatially-defined magnitude, and a dozen gene sets with region-specific activity encoded in specialized neuronal subpopulations. We establish a CAS for each mouse and region, analyzing its trajectory and rate of change over time as a quantitative measure of a region's transcriptional age. Across analyses, white matter and white matter-rich regions emerge as the most transcriptionally impacted areas during aging. It will be particularly interesting to explore how these changes relate to developmental patterns of myelination and brain function, and whether susceptibility to brain aging and dysfunction are related to developmental processes.

The advent of single-cell technologies and cell dissociation methods have enabled the exploration of an ever increasing number of cell populations in the brain (*47*), which in turn allows

for cell type-specific characterization of gene expression during aging (*9*). The interplay between cell type and regional niche during aging is, however, yet to be more deeply understood. Our results emphasize the importance of region identity as a profound modulator of gene expression dynamics in the context of aging and neurodegeneration. It will be important for future studies to examine if these heterogeneous expression patterns result in corresponding shifts of the proteome or downstream functional changes in neuronal activity and plasticity. While we established that a common aging signature increased in microglia with region-dependent effect size, we propose further exploration of the CAS in other non-neuronal cell types. This may help clarify if microglia are active drivers of the regional expression dynamics described here, or rather respond to cues provided by other cell type(s) in the region.

Our data reveal that certain brain regions are selectively vulnerable to aging, with the white matter fiber tracts exhibiting a particular sensitivity. These areas are dense with myelinated axons and myelinating cells, forming the basis of neurotransmission across brain regions (*48*). The strong activation of immune- and inflammation-related genes, as well as differential expression of remyelination regulators like *Gpr17* (*49*, *50*), suggest that the homeostasis of this region is compromised at old age. This could perturb myelin sheath integrity and potentially impair axonal signal transmission between regions as an early event in brain aging. In line with this hypothesis, rejuvenation of hippocampal oligodendrogenesis in aged mice via injection of young cerebrospinal fluid (CSF) improves long-term memory consolidation, thus demonstrating a causal role of compromised myelin on cognition (*51*). The region-specific transcriptome atlas generated here can form a basis for testing rejuvenation strategies such as dietary interventions, plasma and CSF-based therapeutics as well as epigenetic reprogramming to quantify their spatiotemporal impact on the brain at the molecular level.

Our findings strongly support the notion that the impacts of aging on brain function are region specific, potentially relating to the regional vulnerability across different diseases as well as the varied manifestations of neurodegeneration at the level of an individual. We demonstrate that key genetic risk genes are differentially expressed in a region-specific manner, thus locally amplifying, or attenuating their impact on disease pathways. Importantly, our findings also suggest that aging may drive dysfunction in brain regions that are not predominantly affected and studied by classical pathological hallmarks, highlighted by AD risk genes including *Apoe*, *Ms4a6d*, *Plcg2* and *Gab2* which are dysregulated with aging in the mouse choroid plexus, corpus callosum and pons with aging. The translation of these findings to humans may serve as a new brain cartography leading to novel treatment strategies and interventions.

References and Notes

1. A. Kalache, A. Gatti, Active ageing: a policy framework. *Adv. Gerontol.* **11**, 7–18 (2003).

2. L. Partridge, J. Deelen, P. E. Slagboom, Facing up to the global challenges of ageing. *Nature*. **561**, 45–56 (2018).

3. C. López-Otín, M. A. Blasco, L. Partridge, M. Serrano, G. Kroemer, The hallmarks of aging. *Cell*. **153**, 1194–1217 (2013).

4. Y. Hou, X. Dan, M. Babbar, Y. Wei, S. G. Hasselbalch, D. L. Croteau, V. A. Bohr, Ageing as a risk factor for neurodegenerative disease. *Nat. Rev. Neurol.* **15**, 565–581 (2019).

5. T. Niccoli, L. Partridge, A. M. Isaacs, Ageing as a risk factor for ALS/FTD. *Hum. Mol. Genet.* **26**, R105–R113 (2017).

6. R. Pomponio, G. Erus, M. Habes, J. Doshi, D. Srinivasan, E. Mamourian, V. Bashyam, I. M. Nasrallah, T. D. Satterthwaite, Y. Fan, L. J. Launer, C. L. Masters, P. Maruff, C. Zhuo, H. Völzke, S. C. Johnson, J. Fripp, N. Koutsouleris, D. H. Wolf, R. Gur, R. Gur, J. Morris, M. S. Albert, H. J. Grabe, S. M. Resnick, R. N. Bryan, D. A. Wolk, R. T. Shinohara, H. Shou, C. Davatzikos, Harmonization of large MRI datasets for the analysis of brain imaging patterns throughout the lifespan. *Neuroimage*. **208**, 116450 (2020).

7. X. Feng, J. Guo, H. C. Sigmon, R. P. Sloan, A. M. Brickman, F. A. Provenzano, S. A. Small, Alzheimer's Disease Neuroimaging Initiative, Brain regions vulnerable and resistant to aging without Alzheimer's disease. *PLoS One*. **15**, e0234255 (2020).

8. N. Schaum, B. Lehallier, O. Hahn, R. Pálovics, S. Hosseinzadeh, S. E. Lee, R. Sit, D. P. Lee, P. M. Losada, M. E. Zardeneta, T. Fehlmann, J. T. Webber, A. McGeever, K. Calcuttawala, H. Zhang, D. Berdnik, V. Mathur, W. Tan, A. Zee, M. Tan, Tabula Muris Consortium, A. O. Pisco, J. Karkanias, N. F. Neff, A. Keller, S. Darmanis, S. R. Quake, T. Wyss-Coray, Ageing hallmarks exhibit organ-specific temporal signatures. *Nature*. **583**, 596–602 (2020).

9. M. T. Buckley, E. Sun, B. M. George, L. Liu, N. Schaum, L. Xu, J. M. Reyes, M. A. Goodell, I. L. Weissman, T. Wyss-Coray, T. A. Rando, A. Brunet, Cell type-specific aging clocks to quantify aging and rejuvenation in regenerative regions of the brain. *bioRxiv* (2022), p. 2022.01.10.475747.

10. C. Colantuoni, B. K. Lipska, T. Ye, T. M. Hyde, R. Tao, J. T. Leek, E. A. Colantuoni, A. G. Elkahloun, M. M. Herman, D. R. Weinberger, J. E. Kleinman, Temporal dynamics and genetic control of transcription in the human prefrontal cortex. *Nature*. **478**, 519–523 (2011).

11. S. Ham, S.-J. V. Lee, Advances in transcriptome analysis of human brain aging. *Exp. Mol. Med.* **52**, 1787–1797 (2020).

12. H. J. Kang, Y. I. Kawasawa, F. Cheng, Y. Zhu, X. Xu, M. Li, A. M. M. Sousa, M. Pletikos,

K. A. Meyer, G. Sedmak, T. Guennel, Y. Shin, M. B. Johnson, Z. Krsnik, S. Mayer, S. Fertuzinhos, S. Umlauf, S. N. Lisgo, A. Vortmeyer, D. R. Weinberger, S. Mane, T. M. Hyde, A. Huttner, M. Reimers, J. E. Kleinman, N. Sestan, Spatio-temporal transcriptome of the human brain. *Nature*. **478**, 483–489 (2011).

13. L. Soreq, UK Brain Expression Consortium, North American Brain Expression Consortium, J. Rose, E. Soreq, J. Hardy, D. Trabzuni, M. R. Cookson, C. Smith, M. Ryten, R. Patani, J. Ule, Major Shifts in Glial Regional Identity Are a Transcriptional Hallmark of Human Brain Aging. *Cell Rep.* **18**, 557–570 (2017).

14. D. Trabzuni, M. Ryten, R. Walker, C. Smith, S. Imran, A. Ramasamy, M. E. Weale, J. Hardy, Quality control parameters on a large dataset of regionally dissected human control brains for whole genome expression studies. *J. Neurochem.* **119**, 275–282 (2011).

15. M. Melé, P. G. Ferreira, F. Reverter, D. S. DeLuca, J. Monlong, M. Sammeth, T. R. Young, J. M. Goldmann, D. D. Pervouchine, T. J. Sullivan, R. Johnson, A. V. Segrè, S. Djebali, A. Niarchou, GTEx Consortium, F. A. Wright, T. Lappalainen, M. Calvo, G. Getz, E. T. Dermitzakis, K. G. Ardlie, R. Guigó, Human genomics. The human transcriptome across tissues and individuals. *Science*. **348**, 660–665 (2015).

16. C. K. Lee, R. Weindruch, T. A. Prolla, Gene-expression profile of the ageing brain in mice. *Nat. Genet.* **25**, 294–297 (2000).

17. J. M. Zahn, S. Poosala, A. B. Owen, D. K. Ingram, A. Lustig, A. Carter, A. T. Weeraratna, D. D. Taub, M. Gorospe, K. Mazan-Mamczarz, E. G. Lakatta, K. R. Boheler, X. Xu, M. P. Mattson, G. Falco, M. S. H. Ko, D. Schlessinger, J. Firman, S. K. Kummerfeld, W. H. Wood 3rd, A. B. Zonderman, S. K. Kim, K. G. Becker, AGEMAP: a gene expression database for aging in mice. *PLoS Genet.* **3**, e201 (2007).

18. K. E. Hargis, E. M. Blalock, Transcriptional signatures of brain aging and Alzheimer's disease: What are our rodent models telling us? *Behav. Brain Res.* **322**, 311–328 (2017).

19. Tabula Muris Consortium, A single-cell transcriptomic atlas characterizes ageing tissues in the mouse. *Nature*. **583**, 590–595 (2020).

20. O. Mueller, RNA Integrity Number (RIN) – Standardization of RNA Quality Control (available at https://www.agilent.com/cs/library/applications/5989-1165EN.pdf).

21. [No title], (available at https://www.10xgenomics.com/resources/datasets/aggregate-of-mouse-brain-sections-visium-fresh-frozen-whole-transcriptome-1-standard).

22. D. DeTomaso, M. G. Jones, M. Subramaniam, T. Ashuach, C. J. Ye, N. Yosef, Functional interpretation of single cell similarity maps. *Nat. Commun.* **10**, 4376 (2019).

23. E. S. Lein, M. J. Hawrylycz, N. Ao, M. Ayres, A. Bensinger, A. Bernard, A. F. Boe, M. S. Boguski, K. S. Brockway, E. J. Byrnes, L. Chen, L. Chen, T.-M. Chen, M. C. Chin, J. Chong, B. E. Crook, A. Czaplinska, C. N. Dang, S. Datta, N. R. Dee, A. L. Desaki, T. Desta, E. Diep, T. A. Dolbeare, M. J. Donelan, H.-W. Dong, J. G. Dougherty, B. J. Duncan, A. J. Ebbert, G. Eichele, L. K. Estin, C. Faber, B. A. Facer, R. Fields, S. R. Fischer, T. P.

Fliss, C. Frensley, S. N. Gates, K. J. Glattfelder, K. R. Halverson, M. R. Hart, J. G. Hohmann, M. P. Howell, D. P. Jeung, R. A. Johnson, P. T. Karr, R. Kawal, J. M. Kidney, R. H. Knapik, C. L. Kuan, J. H. Lake, A. R. Laramee, K. D. Larsen, C. Lau, T. A. Lemon, A. J. Liang, Y. Liu, L. T. Luong, J. Michaels, J. J. Morgan, R. J. Morgan, M. T. Mortrud, N. F. Mosqueda, L. L. Ng, R. Ng, G. J. Orta, C. C. Overly, T. H. Pak, S. E. Parry, S. D. Pathak, O. C. Pearson, R. B. Puchalski, Z. L. Riley, H. R. Rockett, S. A. Rowland, J. J. Royall, M. J. Ruiz, N. R. Sarno, K. Schaffnit, N. V. Shapovalova, T. Sivisay, C. R. Slaughterbeck, S. C. Smith, K. A. Smith, B. I. Smith, A. J. Sodt, N. N. Stewart, K.-R. Stumpf, S. M. Sunkin, M. Sutram, A. Tam, C. D. Teemer, C. Thaller, C. L. Thompson, L. R. Varnam, A. Visel, R. M. Whitlock, P. E. Wohnoutka, C. K. Wolkey, V. Y. Wong, M. Wood, M. B. Yaylaoglu, R. C. Young, B. L. Youngstrom, X. F. Yuan, B. Zhang, T. A. Zwingman, A. R. Jones, Genome-wide atlas of gene expression in the adult mouse brain. *Nature*. **445**, 168–176 (2007).

24. B. W. Dulken, M. T. Buckley, P. Navarro Negredo, N. Saligrama, R. Cayrol, D. S. Leeman, B. M. George, S. C. Boutet, K. Hebestreit, J. V. Pluvinage, T. Wyss-Coray, I. L. Weissman, H. Vogel, M. M. Davis, A. Brunet, Single-cell analysis reveals T cell infiltration in old neurogenic niches. *Nature*. **571**, 205–210 (2019).

25. A. Sekar, A. R. Bialas, H. de Rivera, A. Davis, T. R. Hammond, N. Kamitaki, K. Tooley, J. Presumey, M. Baum, V. Van Doren, G. Genovese, S. A. Rose, R. E. Handsaker, Schizophrenia Working Group of the Psychiatric Genomics Consortium, M. J. Daly, M. C. Carroll, B. Stevens, S. A. McCarroll, Schizophrenia risk from complex variation of complement component 4. *Nature*. **530**, 177–183 (2016).

26. O. Hahn, T. Fehlmann, H. Zhang, C. N. Munson, R. T. Vest, A. Borcherding, S. Liu, C. Villarosa, S. Drmanac, R. Drmanac, A. Keller, T. Wyss-Coray, CoolMPS for robust sequencing of single-nuclear RNAs captured by droplet-based method. *Nucleic Acids Res.* (2020), doi:10.1093/nar/gkaa1127.

27. Y. Zhou, W. M. Song, P. S. Andhey, A. Swain, T. Levy, K. R. Miller, P. L. Poliani, M. Cominelli, S. Grover, S. Gilfillan, M. Cella, T. K. Ulland, K. Zaitsev, A. Miyashita, T. Ikeuchi, M. Sainouchi, A. Kakita, D. A. Bennett, J. A. Schneider, M. R. Nichols, S. A. Beausoleil, J. D. Ulrich, D. M. Holtzman, M. N. Artyomov, M. Colonna, Human and mouse single-nucleus transcriptomics reveal TREM2-dependent and TREM2-independent cellular responses in Alzheimer's disease. *Nat. Med.* **26**, 131–142 (2020).

28. M. Ximerakis, S. L. Lipnick, B. T. Innes, S. K. Simmons, X. Adiconis, D. Dionne, B. A. Mayweather, L. Nguyen, Z. Niziolek, C. Ozek, V. L. Butty, R. Isserlin, S. M. Buchanan, S. S. Levine, A. Regev, G. D. Bader, J. Z. Levin, L. L. Rubin, Single-cell transcriptomic profiling of the aging mouse brain. *Nat. Neurosci.* **22**, 1696–1708 (2019).

29. N. C. Berchtold, D. H. Cribbs, P. D. Coleman, J. Rogers, E. Head, R. Kim, T. Beach, C. Miller, J. Troncoso, J. Q. Trojanowski, H. R. Zielke, C. W. Cotman, Gene expression changes in the course of normal brain aging are sexually dimorphic. *Proc. Natl. Acad. Sci. U. S. A.* **105**, 15605–15610 (2008).

30. G. W. Van Hoesen, B. T. Hyman, A. R. Damasio, Entorhinal cortex pathology in

Alzheimer's disease. *Hippocampus*. **1**, 1–8 (1991).

31. P. Langfelder, S. Horvath, WGCNA: an R package for weighted correlation network analysis. *BMC Bioinformatics*. **9**, 559 (2008).

32. W.-T. Chen, A. Lu, K. Craessaerts, B. Pavie, C. Sala Frigerio, N. Corthout, X. Qian, J. Laláková, M. Kühnemund, I. Voytyuk, L. Wolfs, R. Mancuso, E. Salta, S. Balusu, A. Snellinx, S. Munck, A. Jurek, J. Fernandez Navarro, T. C. Saido, I. Huitinga, J. Lundeberg, M. Fiers, B. De Strooper, Spatial Transcriptomics and In Situ Sequencing to Study Alzheimer's Disease. *Cell*. **182**, 976–991.e19 (2020).

33. J. V. Pluvinage, M. S. Haney, B. A. H. Smith, J. Sun, T. Iram, L. Bonanno, L. Li, D. P. Lee, D. W. Morgens, A. C. Yang, S. R. Shuken, D. Gate, M. Scott, P. Khatri, J. Luo, C. R. Bertozzi, M. C. Bassik, T. Wyss-Coray, CD22 blockade restores homeostatic microglial phagocytosis in ageing brains. *Nature*. **568**, 187–192 (2019).

34. F. L. Yeh, D. V. Hansen, M. Sheng, TREM2, Microglia, and Neurodegenerative Diseases. *Trends Mol. Med.* **23**, 512–533 (2017).

35. Y. Yuan, Y.-P. P. Chen, J. Boyd-Kirkup, P. Khaitovich, M. Somel, Accelerated aging-related transcriptome changes in the female prefrontal cortex. *Aging Cell*. **11**, 894–901 (2012).

36. M. M. Corrada, R. Brookmeyer, D. Berlau, A. Paganini-Hill, C. H. Kawas, Prevalence of dementia after age 90: results from the 90+ study. *Neurology*. **71**, 337–343 (2008).

37. K. Mozhui, L. Lu, W. E. Armstrong, R. W. Williams, Sex-specific modulation of gene expression networks in murine hypothalamus. *Front. Neurosci.* **6**, 63 (2012).

38. S. Yamagishi, F. Hampel, K. Hata, D. Del Toro, M. Schwark, E. Kvachnina, M. Bastmeyer, T. Yamashita, V. Tarabykin, R. Klein, J. Egea, FLRT2 and FLRT3 act as repulsive guidance cues for Unc5-positive neurons. *EMBO J.* **30**, 2920–2933 (2011).

39. W. Wu, S. E. Hill, W. J. Nathan, J. Paiano, E. Callen, D. Wang, K. Shinoda, N. van Wietmarschen, J. M. Colón-Mercado, D. Zong, R. De Pace, H.-Y. Shih, S. Coon, M. Parsadanian, R. Pavani, H. Hanzlikova, S. Park, S. K. Jung, P. J. McHugh, A. Canela, C. Chen, R. Casellas, K. W. Caldecott, M. E. Ward, A. Nussenzweig, Neuronal enhancers are hotspots for DNA single-strand break repair. *Nature*. **593**, 440–444 (2021).

40. E. Brouillet, B. G. Jenkins, B. T. Hyman, R. J. Ferrante, N. W. Kowall, R. Srivastava, D. S. Roy, B. R. Rosen, M. F. Beal, Age-dependent vulnerability of the striatum to the mitochondrial toxin 3-nitropropionic acid. *J. Neurochem.* **60**, 356–359 (1993).

41. G. Patki, Y. Che, Y.-S. Lau, Mitochondrial dysfunction in the striatum of aged chronic mouse model of Parkinson's disease. *Front. Aging Neurosci.* **1**, 3 (2009).

42. A. C. Yang, F. Kern, P. M. Losada, M. R. Agam, C. A. Maat, G. P. Schmartz, T. Fehlmann, J. A. Stein, N. Schaum, D. P. Lee, K. Calcuttawala, R. T. Vest, D. Berdnik, N. Lu, O. Hahn, D. Gate, M. W. McNerney, D. Channappa, I. Cobos, N. Ludwig, W. J. Schulz-Schaeffer, A.

Keller, T. Wyss-Coray, Dysregulation of brain and choroid plexus cell types in severe COVID-19. *Nature*. **595**, 565–571 (2021).

43. A. C. Yang, R. T. Vest, F. Kern, D. P. Lee, M. Agam, C. A. Maat, P. M. Losada, M. B. Chen, N. Schaum, N. Khoury, A. Toland, K. Calcuttawala, H. Shin, R. Pálovics, A. Shin, E. Y. Wang, J. Luo, D. Gate, W. J. Schulz-Schaeffer, P. Chu, J. A. Siegenthaler, M. W. McNerney, A. Keller, T. Wyss-Coray, A human brain vascular atlas reveals diverse mediators of Alzheimer's risk. *Nature*. **603**, 885–892 (2022).

44. Y. Kihara, Y. Zhu, D. Jonnalagadda, W. Romanow, C. Palmer, B. Siddoway, R. Rivera, R. Dutta, B. D. Trapp, J. Chun, Single-Nucleus RNA-seq of Normal-Appearing Brain Regions in Relapsing-Remitting vs. Secondary Progressive Multiple Sclerosis: Implications for the Efficacy of Fingolimod. *Front. Cell. Neurosci.* **16**, 918041 (2022).

45. E. M. Reiman, J. A. Webster, A. J. Myers, J. Hardy, T. Dunckley, V. L. Zismann, K. D. Joshipura, J. V. Pearson, D. Hu-Lince, M. J. Huentelman, D. W. Craig, K. D. Coon, W. S. Liang, R. H. Herbert, T. Beach, K. C. Rohrer, A. S. Zhao, D. Leung, L. Bryden, L. Marlowe, M. Kaleem, D. Mastroeni, A. Grover, C. B. Heward, R. Ravid, J. Rogers, M. L. Hutton, S. Melquist, R. C. Petersen, G. E. Alexander, R. J. Caselli, W. Kukull, A. Papassotiropoulos, D. A. Stephan, GAB2 alleles modify Alzheimer's risk in APOE epsilon4 carriers. *Neuron*. **54**, 713–720 (2007).

46. L. Nagpal, M. D. Kornberg, S. H. Snyder, Inositol hexakisphosphate kinase-2 non-catalytically regulates mitophagy by attenuating PINK1 signaling. *Proc. Natl. Acad. Sci. U. S. A.* **119**, e2121946119 (2022).

47. BRAIN Initiative Cell Census Network (BICCN), A multimodal cell census and atlas of the mammalian primary motor cortex. *Nature*. **598**, 86–102 (2021).

48. H. Liu, Y. Yang, Y. Xia, W. Zhu, R. K. Leak, Z. Wei, J. Wang, X. Hu, Aging of cerebral white matter. *Ageing Res. Rev.* **34**, 64–76 (2017).

49. A. Dziedzic, E. Miller, J. Saluk-Bijak, M. Bijak, The GPR17 Receptor-A Promising Goal for Therapy and a Potential Marker of the Neurodegenerative Process in Multiple Sclerosis. *Int. J. Mol. Sci.* **21** (2020), doi:10.3390/ijms21051852.

50. A. D. Rivera, F. Pieropan, I. Chacon-De-La-Rocha, D. Lecca, M. P. Abbracchio, K. Azim, A. M. Butt, Functional genomic analyses highlight a shift in Gpr17-regulated cellular processes in oligodendrocyte progenitor cells and underlying myelin dysregulation in the aged mouse cerebrum. *Aging Cell*. **20**, e13335 (2021).

51. T. Iram, F. Kern, A. Kaur, S. Myneni, A. R. Morningstar, H. Shin, M. A. Garcia, L. Yerra, R. Palovics, A. C. Yang, O. Hahn, N. Lu, S. R. Shuken, M. S. Haney, B. Lehallier, M. Iyer, J. Luo, H. Zetterberg, A. Keller, J. B. Zuchero, T. Wyss-Coray, Young CSF restores oligodendrogenesis and memory in aged mice via Fgf17. *Nature*. **605**, 509–515 (2022).

52. J. Wager-Miller, M. Murphy Green, H. Shafique, K. Mackie, Collection of Frozen Rodent Brain Regions for Downstream Analyses. *J. Vis. Exp.* (2020), doi:10.3791/60474.

53. Z. De Miguel, N. Khoury, M. J. Betley, B. Lehallier, D. Willoughby, N. Olsson, A. C. Yang, O. Hahn, N. Lu, R. T. Vest, L. N. Bonanno, L. Yerra, L. Zhang, N. L. Saw, J. K. Fairchild, D. Lee, H. Zhang, P. L. McAlpine, K. Contrepois, M. Shamloo, J. E. Elias, T. A. Rando, T. Wyss-Coray, Exercise plasma boosts memory and dampens brain inflammation via clusterin. *Nature*. **600**, 494–499 (2021).

54. Babraham Bioinformatics - SeqMonk Mapped Sequence Analysis Tool, (available at http://www.bioinformatics.babraham.ac.uk/projects/seqmonk/).

55. RStudio, (available at https://www.rstudio.com/).

56. M. I. Love, W. Huber, S. Anders, Moderated estimation of fold change and dispersion for RNA-seq data with DESeq2. *Genome Biol.* **15**, 550 (2014).

57. T. Stuart, A. Butler, P. Hoffman, C. Hafemeister, E. Papalexi, W. M. Mauck 3rd, Y. Hao, M. Stoeckius, P. Smibert, R. Satija, Comprehensive Integration of Single-Cell Data. *Cell*. **177**, 1888–1902.e21 (2019).

58. *CellPlot: R package for the integrated visualisation of functional enrichment and expression data* (Github; https://github.com/dieterich-lab/CellPlot).

59. M. Ferreira, S. Francisco, A. R. Soares, A. Nobre, M. Pinheiro, A. Reis, S. Neto, A. J. Rodrigues, N. Sousa, G. Moura, M. A. S. Santos, Integration of segmented regression analysis with weighted gene correlation network analysis identifies genes whose expression is remodeled throughout physiological aging in mouse tissues. *Aging* . **13**, 18150–18190 (2021).

60. T. Goldmann, P. Wieghofer, M. J. C. Jordão, F. Prutek, N. Hagemeyer, K. Frenzel, L. Amann, O. Staszewski, K. Kierdorf, M. Krueger, G. Locatelli, H. Hochgerner, R. Zeiser, S. Epelman, F. Geissmann, J. Priller, F. M. V. Rossi, I. Bechmann, M. Kerschensteiner, S. Linnarsson, S. Jung, M. Prinz, Origin, fate and dynamics of macrophages at central nervous system interfaces. *Nat. Immunol.* **17**, 797–805 (2016).

61. A. Zeisel, A. B. Muñoz-Manchado, S. Codeluppi, P. Lönnerberg, G. La Manno, A. Juréus, S. Marques, H. Munguba, L. He, C. Betsholtz, C. Rolny, G. Castelo-Branco, J. Hjerling-Leffler, S. Linnarsson, Brain structure. Cell types in the mouse cortex and hippocampus revealed by single-cell RNA-seq. *Science*. **347**, 1138–1142 (2015).

62. Y. Zhang, S. A. Sloan, L. E. Clarke, C. Caneda, C. A. Plaza, P. D. Blumenthal, H. Vogel, G. K. Steinberg, M. S. B. Edwards, G. Li, J. A. Duncan 3rd, S. H. Cheshier, L. M. Shuer, E. F. Chang, G. A. Grant, M. G. H. Gephart, B. A. Barres, Purification and Characterization of Progenitor and Mature Human Astrocytes Reveals Transcriptional and Functional Differences with Mouse. *Neuron*. **89**, 37–53 (2016).

63. R. Pálovics, A. Keller, N. Schaum, W. Tan, T. Fehlmann, M. Borja, F. Kern, L. Bonanno, K. Calcuttawala, J. Webber, A. McGeever, Tabula Muris Consortium, J. Luo, A. O. Pisco,

J. Karkanias, N. F. Neff, S. Darmanis, S. R. Quake, T. Wyss-Coray, Molecular hallmarks of heterochronic parabiosis at single-cell resolution. *Nature*. **603**, 309–314 (2022).

64. R. V. Lenth, Least-Squares Means: The R Package lsmeans. *J. Stat. Softw.* **69**, 1–33 (2016).

65. H. Mathys, J. Davila-Velderrain, Z. Peng, F. Gao, S. Mohammadi, J. Z. Young, M. Menon, L. He, F. Abdurrob, X. Jiang, A. J. Martorell, R. M. Ransohoff, B. P. Hafler, D. A. Bennett, M. Kellis, L.-H. Tsai, Single-cell transcriptomic analysis of Alzheimer's disease. *Nature*. **570**, 332–337 (2019).

66. S. Picelli, Å. K. Björklund, O. R. Faridani, S. Sagasser, G. Winberg, R. Sandberg, Smart-seq2 for sensitive full-length transcriptome profiling in single cells. *Nat. Methods*. **10**, 1096–1098 (2013).

67. G. Finak, A. McDavid, M. Yajima, J. Deng, V. Gersuk, A. K. Shalek, C. K. Slichter, H. W. Miller, M. J. McElrath, M. Prlic, P. S. Linsley, R. Gottardo, MAST: a flexible statistical framework for assessing transcriptional changes and characterizing heterogeneity in single-cell RNA sequencing data. *Genome Biol.* **16**, 278 (2015).

Acknowledgments: We thank the members of the Wyss-Coray laboratory for feedback and support, and H. Zhang, D. Berdnik, K. Dickey and D. Channappa for laboratory management. We further thank the Neuroscience Microscopy Service center and director G. Wang for microscopy training and assistance in acquiring images for Spatial-seq. We thank A. Bastian for advice in establishing the Spatial-seq experiments.

Funding:

Schaller-Nikolich Foundation (A.Ke.)

Wu Tsai Neurosciences Institute and Bertarelli Foundation (T.W.-C.)

Cure Alzheimer's Fund (T.W.-C.)

National Institute of Aging grant R01-AG072255 (T.W.-C.)

The Milky Way Research Foundation (T.W.-C.)

The American Heart Association-Allen Initiative in Brain Health and Cognitive Impairment (T.W.-C.)

The Phil and Penny Knight Initiative for Brain Resilience (T.W.-C.)

Michael J. Fox Foundation for Parkinson's Research grant 125491594 (A.Ke and F.K.)

Michael J. Fox Foundation for Parkinson's Research grant MJFF-021418 (T.W.-C., A.Ke. and F.K.).

Author contributions: O.H. and T.W.-C. conceptualized the study. O.H. designed and led experiments, conducted bioinformatic analyses and prepared the manuscript. A.G.F. and O.H. selected regions and devised the brain dissociation method. J.H. and J.R.H aided in region selection and method design. O.H., I.H.G., C.M., A.G.F., M.A., B.K. and A.Ka. conducted the tissue collection. A.G.F. dissociated and organized brain regions, and extracted RNA. N.L. and O.H. established the bulk-seq workflow. A.G.F., M.A. and O.H. processed libraries for bulk-seq. B.K. and O.H. conducted the Spatial-seq experiments. I.H.G., C.M. and A.Ka. aided with the H&E workflow. M.A. and A.G.F. performed the nuc-seq experiments. P.M.L., B.L., R.P., F.K. and A.Ke. assisted with analysis and bioinformatics procedures. B.K. developed the searchable web interface (Shiny app). O.H. and T.W.-C. edited the manuscript with input from all authors. All authors read and approved the final manuscript.

Competing interests: The authors declare no competing interests.

Data and materials availability: The sequencing datasets analyzed during the current study are available in the Gene Expression Omnibus repository under accession numbers GSE212336, GSE212576 and GSE212903.

Supplementary Materials

Materials and Methods

Figures S1-S11

Data S1-S10

References (52-67)

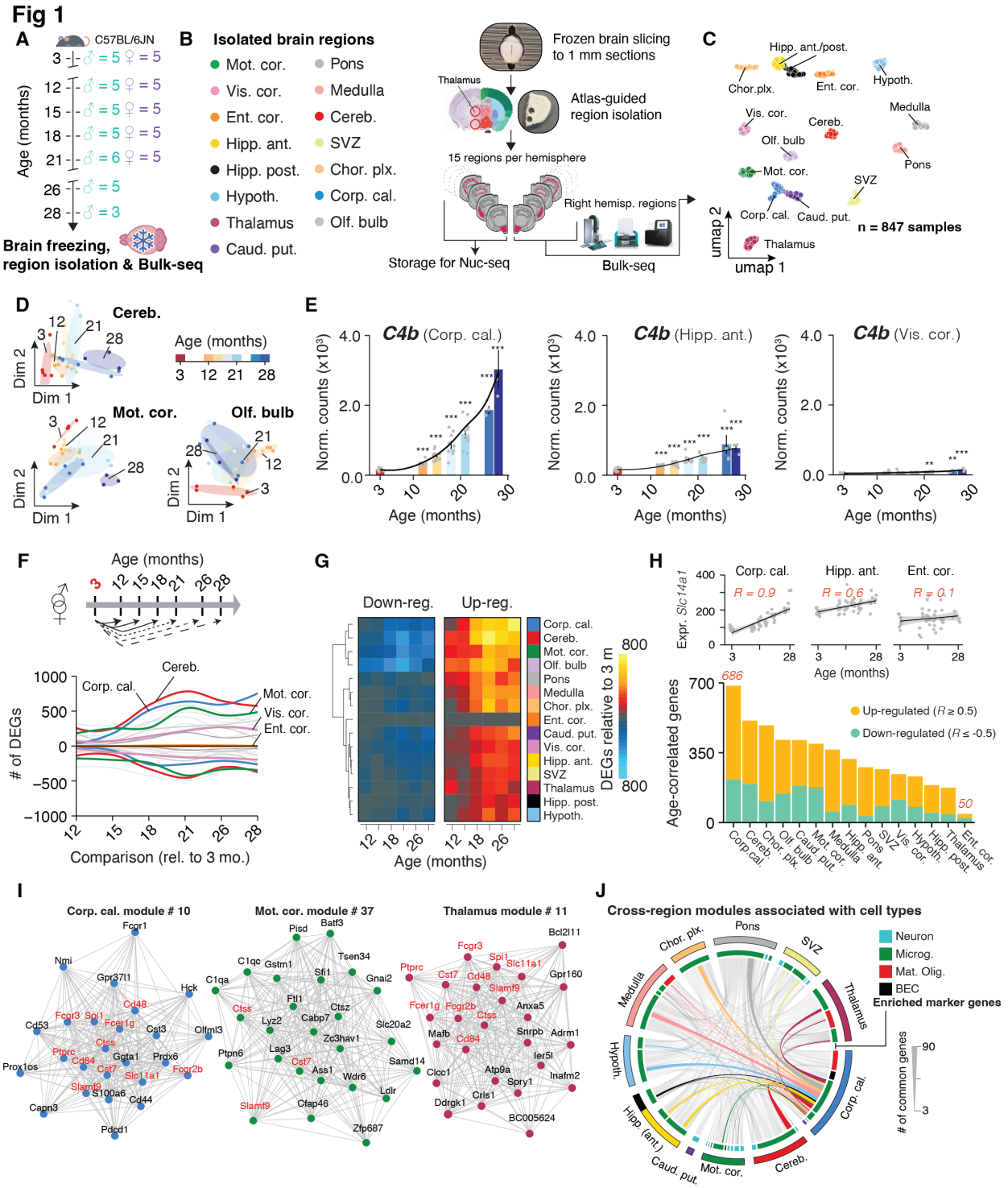

Fig. 1 Brain regions exhibit distinct transcriptional patterns of aging independent of anatomical proximity

(A) Cohort overview. Whole brains were collected from male (n = 3-5, 3–28 months) and female (n = 5, 3–21 months) C57BL/6JN mice. (B) Study outline. 15 brain regions were isolated from each hemisphere of the brains collected in (A). Regions from the right hemisphere were analyzed using Bulk-seq. (C) UMAP representation of brain region transcriptomes (n = 847 total samples), based on the first 40 principal components. (D) Diffusion maps of region transcriptomes from male cerebellum, motor cortex, and olfactory bulb. Dim., dimension. (E) *C4b* expression in corpus callosum, anterior hippocampus and visual cortex. Black lines indicate averaged-smoothed gene expression. Differential expression relative to the 3 months group is indicated. Data are mean ± s.e.m. Two-sided Wald test, adjusted for multiple testing. *** $p < 0.001$, ** $p < 0.01$, * $p < 0.05$. (F) Smoothed line plot displaying the number of DEGs for pairwise comparisons, referenced to data at 3 months. Positive (negative) values represent upregulated (downregulated) genes, gray lines represent non-labelled regions. DEGs that reached significance in ≥ 2 pairwise comparisons were included. (G) Heat map of the data in (F). (H) Number of genes that significantly correlate with age (Spearman's rho ≥ 0.5), colored by up- and down-regulation. (I) Networks of the most highly connected genes ('eigengenes') of three exemplary modules with significant age-association identified in corpus callosum, motor cortex and thalamus. Networks display connections of the corresponding topological overlap above a threshold of 0.08. (J) Chord diagram representation of genes shared in age-associated modules across regions. Modules with significant enrichment of cell type markers are displayed. Modules and associated genes are listed in data S4.

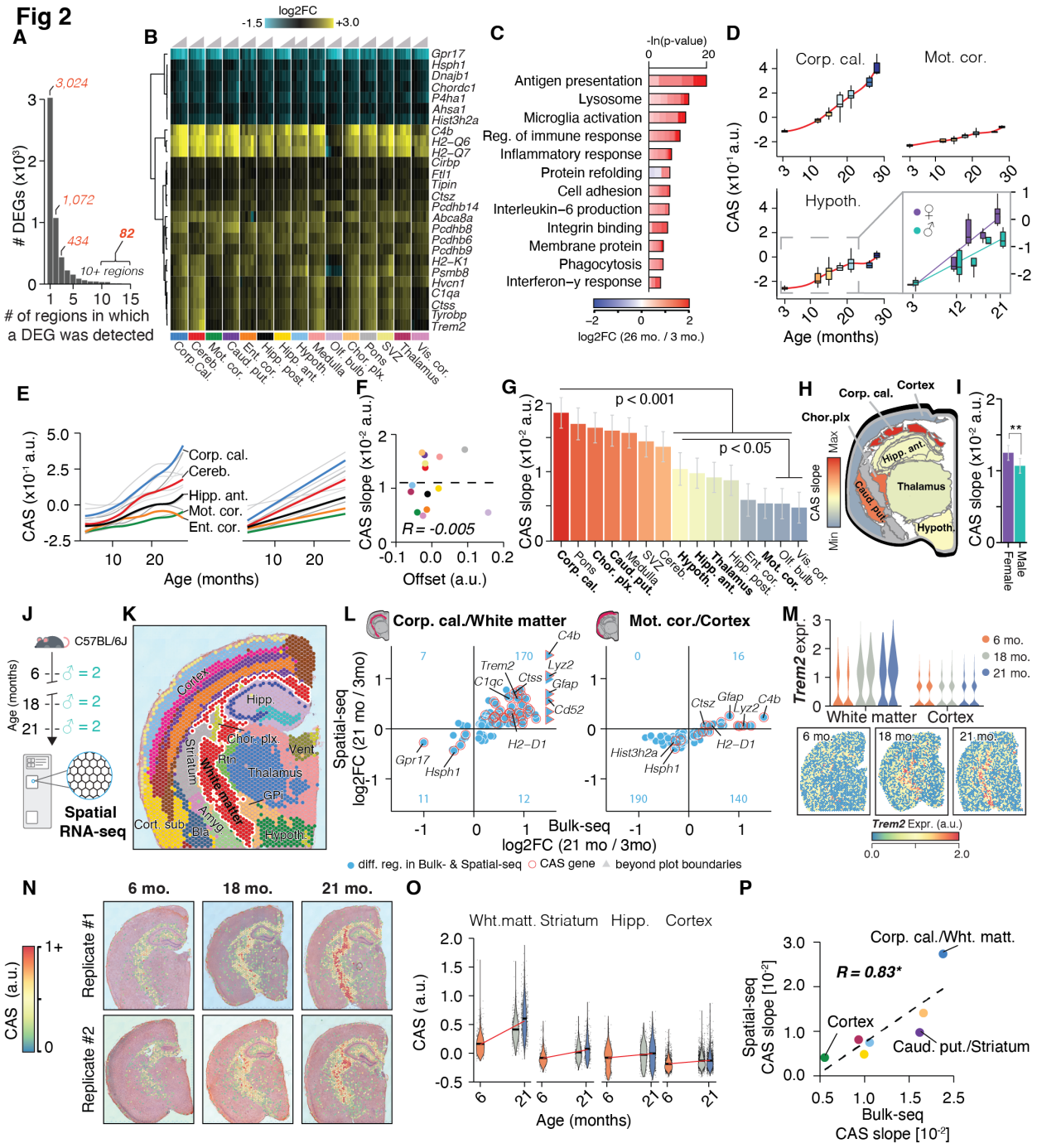

Fig. 2 A common gene signature detects accelerated aging in white matter tracts

(A) Bar graph indicating the number of regions in which a given DEG was detected (data S2). (B) Region-wise expression changes with age (column-wise from left to right) for genes with shifts in at least 10 of the 15 collected regions. (C) Representative GO analysis of 82 genes with shifts in at least 10 of the 15 collected regions that make up the CAS. Lengths of bars represent negative

ln-transformed Padj using two-sided Fisher's exact test. Colors indicate gene-wise log2 fold-changes (log2(FC)) between 26 and 3 months old mice as measured in the corpus callosum. Numbers beside bars indicate differentially expressed genes in that GO category. The complete list of enriched GO terms can be found in data S5. (D) CAS trajectories in the corpus callosum, motor cortex, and hypothalamus. Insert indicates trajectories for male and females in the hypothalamus from 3 to 21 months. (E) CAS trajectories of all regions approximated via local estimate (LOESS) and linear regression, colored by region; gray lines represent non-labelled regions. (F) Offset and slope comparison for linear models in (E), colored by region. Linear regression (dashed line) and Spearman correlation coefficient are indicated. (G) Slope of linear regressions in (D), colored by slope. Data are mean ± 95% confidence intervals. Bolded regions are highlighted in the following panel. (H) Coronal cross-section sketch of the mouse brain, with regions colored according to CAS linear slopes. Corpus callosum was chosen to represent white matter tracts. (I) Slope of linear regression across all brain regions from 3 to 21 months, colored by sex. Data are mean ± 95% confidence intervals. Two-sided Tukey's HSD test, adjusted for multiple testing, *** $p < 0.001$, ** $p < 0.01$, * $p < 0.05$. The highest (least significant) Pval is indicated. (J) Spatial-seq experiment overview. Brain tissue was collected from an independent male C57BL/6J mouse cohort (n = 2 mice; 6, 18 and 21 months). (K) Representative spatial transcriptome data (6 months replicate #2), colored by cluster-based annotation, according to Fig S5. Labels represent region-level annotation according to Fig S5. Complete data description and abbreviations are in Fig S5. (L) Comparison of Bulk- and Spatial-seq differential expression results in white matter cluster/corpus callosum punch; cortex cluster/motor cortex punch. DEGs (Padj < 0.05) found in both datasets are shown, with their log2-transformed expression ratios (21 rel. to 3 months) in Bulk- and Spatial-seq data. CAS genes are highlighted. The number of overlapping DEGs in each quadrant is indicated in blue. (M) Spatially-resolved expression of *Trem2* across

age. Violin plots represent expression in white matter- and cortex-associated spots, split by replicates. (N) Spatial representation of CAS. Spots with values ≥ 0 are shown. (O) Violin plot representing CAS across spatial clusters of white matter, striatum, hippocampus and cortex. Red line indicates linear regression fit. (P) Comparison of CAS slopes for linear models in Bulk- and Spatial-seq, colored by region. Linear regression (dashed line) and Spearman correlation coefficient are indicated. Corpus callosum, caudate putamen and motor cortex regions were chosen to represent white matter, striatum and cortex, respectively.

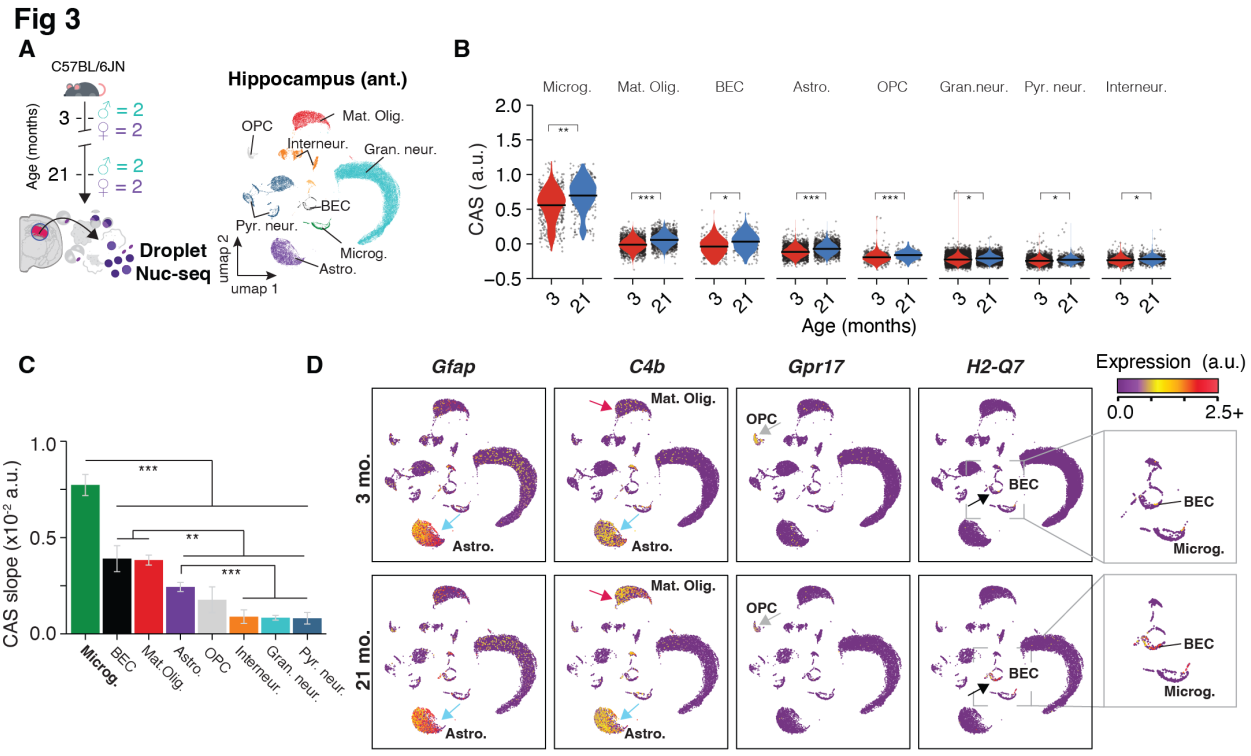

Fig. 3 Aging in glia and endothelial cells is the major contributor to CAS increase

(A) Nuc-seq experiment overview. Nuc-seq of left-hemisphere regions of the anterior hippocampus from the same mice used for bulk RNA-seq (n = 2 males, n = 2 females; 3, and 21 months). UMAP representation of all nuclei populations (n = 36,339 cells). (B) Violin plot representing CAS across hippocampal cell types. Points indicate nuclei-wise expression levels, and the violin indicates average distribution of expression split by age. *P* values calculated with two-tailed t-test on per-replicate median of CAS, adjusted for multiple testing. *** $p < 0.001$, ** $p < 0.01$, * $p < 0.05$ (C) CAS slope of linear regressions in (B), colored by cell type. Data are mean ± 95% confidence intervals. Two-sided Tukey's HSD test, adjusted for multiple testing, *** $p < 0.001$, ** $p < 0.01$, * $p < 0.05$. The highest (least significant) Pval is indicated. (D) Expression of CAS genes *Gfap*, *C4b*, *Gpr17* and *H2-Q7*. Quantification and statistical analysis can be found in Figs. S6 and S7.

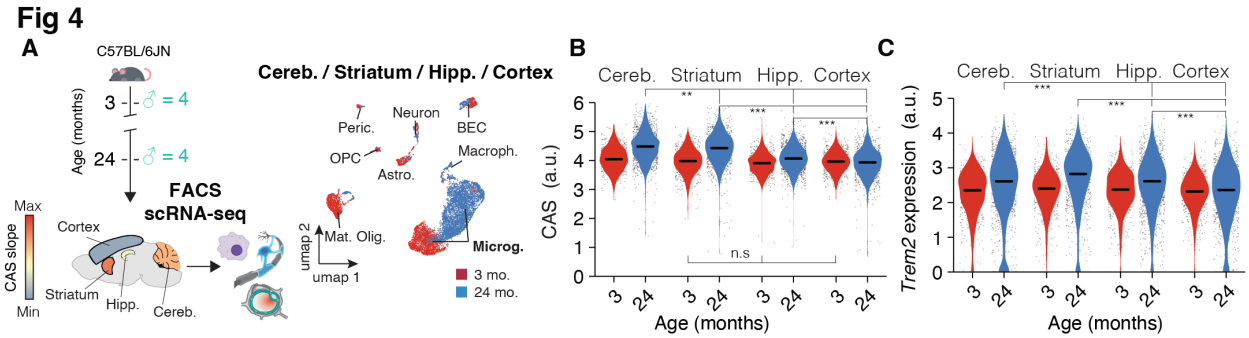

Fig. 4 CAS analysis reveals that transcriptional aging of microglia depends on their region of origin.

(A) Meta-analysis of scRNA-seq data from (*19*) of microglia from cerebellum, striatum, hippocampus and cortex. UMAP representation of all cell populations (n = 6,373 cells), colored by age. Regions are colored according to CAS slopes in Fig. 2G. (B,C) Violin plot representing (B) CAS and (C) *Trem2* expression across microglia from four different brain regions. Points indicate nuclei-wise expression levels, and the violin indicates average distribution of expression split by age. (MAST, Benjamini–Hochberg correction; false discovery rate (FDR) < 0.05 and logFC > 0.2 to be significant). *** $p < 0.001$, ** $p < 0.01$, * $p < 0.05$.

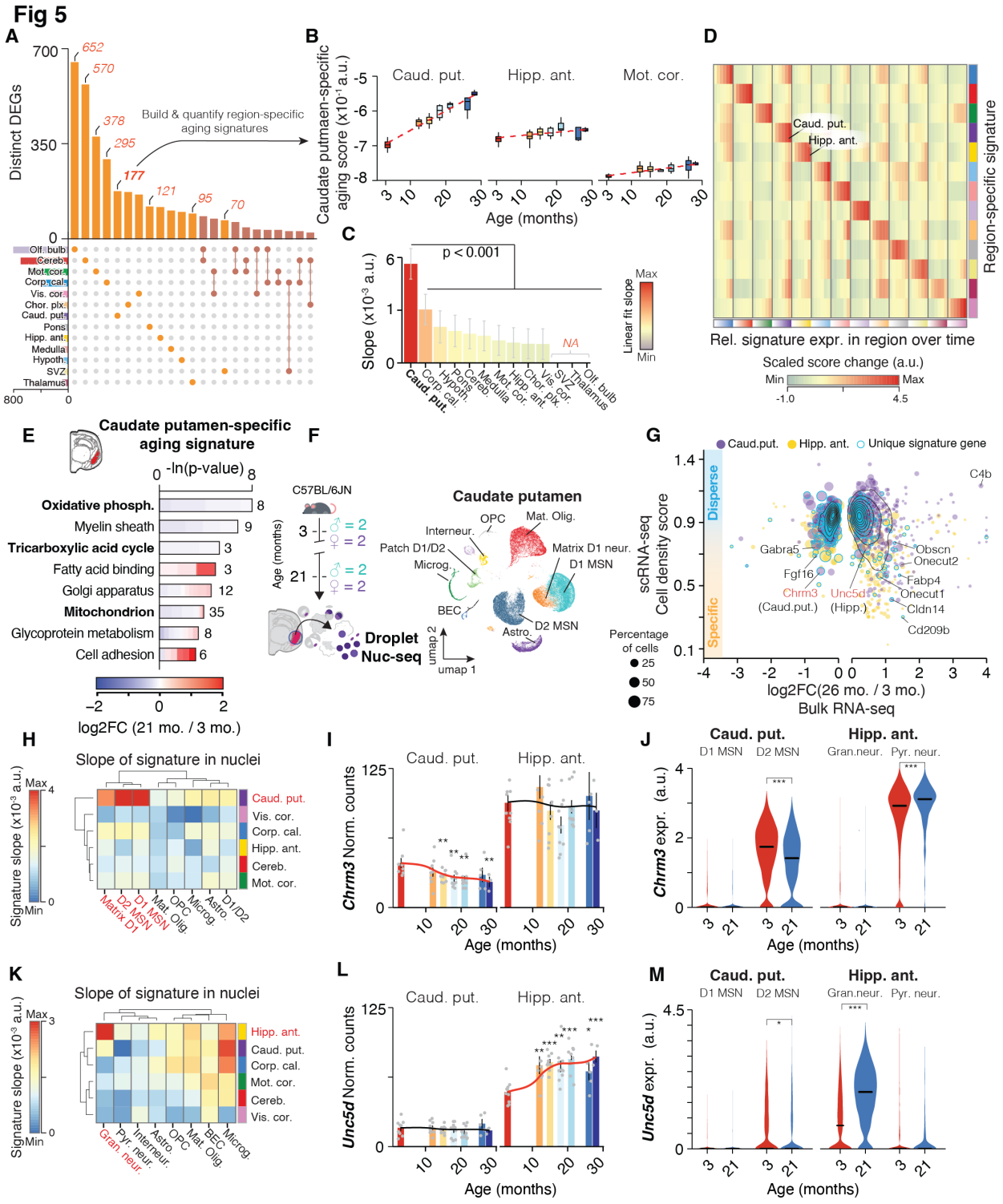

Fig. 5 Region-specific expression shifts are encoded by neuronal transcripts

(A) Regional specificity of DEGs. UpSet plot showing a matrix layout of DEGs shared across and specific to each region. Each matrix column represents either DEGs specific to a region (single

circle with no vertical lines) or DEGs shared between regions, with the vertical line indicating the regions that share that given DEG. Top, bar graph displays the number of DEGs in each combination of regions. Left bottom, bar graph displays the total number of DEGs for a given region. Gene sets with ≥ 25 genes are shown. Unique gene sets were used to construct region-specific aging signatures. (B) Trajectories of caudate putamen-specific aging score in the caudate putamen, anterior hippocampus and motor cortex. Linear fit is indicated as dashed lines. (C) Slope of linear regressions in (B), colored by slope. Data are mean ± 95% confidence intervals. Two-sided Tukey's HSD test, adjusted for multiple testing, *** $p < 0.001$, ** $p < 0.01$, * $p < 0.05$. The highest (least significant) Pval is indicated. (D) Region-wise score changes with age relative to 3 months (column-wise from left to right) for region-specific signatures. Score changes are z-scaled within a row. Quantification and statistical analysis can be found in Fig S10. (E) Representative GO enrichment as in (Fig. 2C) for 177 DEGs unique to the caudate putamen that make up its specific signature. The complete list of enriched GO terms can be found in data S8. (F) Nuc-seq experiment overview. Nuc-seq of left-hemisphere regions of the caudate putamen from the same mice used for bulk RNA-seq (n = 2 males, n = 2 females; 3, and 21 months). UMAP representation of all nuclei populations (n = 45,277 cells). (G) Single-nuclei dispersion scores plotted against log2-transformed expression ratios between 21 and 3 months (bulk RNA-seq) for the caudate putamen and anterior hippocampus. The colors represent different organ types and size of the dots corresponds to the percentage of cells that express a given gene. Genes that make up the region-specific score are highlighted. (H) Slope of cell type-wise changes with age for representative region-specific signatures from (D). D1 and D2 Medium spiny neuron populations (MSN) are highlighted, as they exhibit a distinct increase with age exclusively for the caudate putamen-specific signature. (I) Bulk expression across caudate putamen and anterior hippocampus for *Chrm3*. Black lines indicate averaged-smoothed gene expression. The trajectory with significant

age effect is highlighted. Data are mean ± s.e.m. (J) Violin plot representing *Chrm3* expression across neuronal cell types in caudate putamen and anterior hippocampus. Points indicate nuclei-wise expression levels, and the violin indicates average distribution of expression split by age. (MAST, Benjamini–Hochberg correction; false discovery rate (FDR) < 0.05 and logFC > 0.2 to be significant). *** $p < 0.001$, ** $p < 0.01$, * $p < 0.05$. (K) Slope of cell type-wise changes with age for representative region-specific signatures from (D). Granule cells are highlighted, as they exhibit a distinct increase with age exclusively for the anterior hippocampus-specific signature. (L) Same as (I) for *Unc5d*. (M) Same as (J) for *Unc5d*.

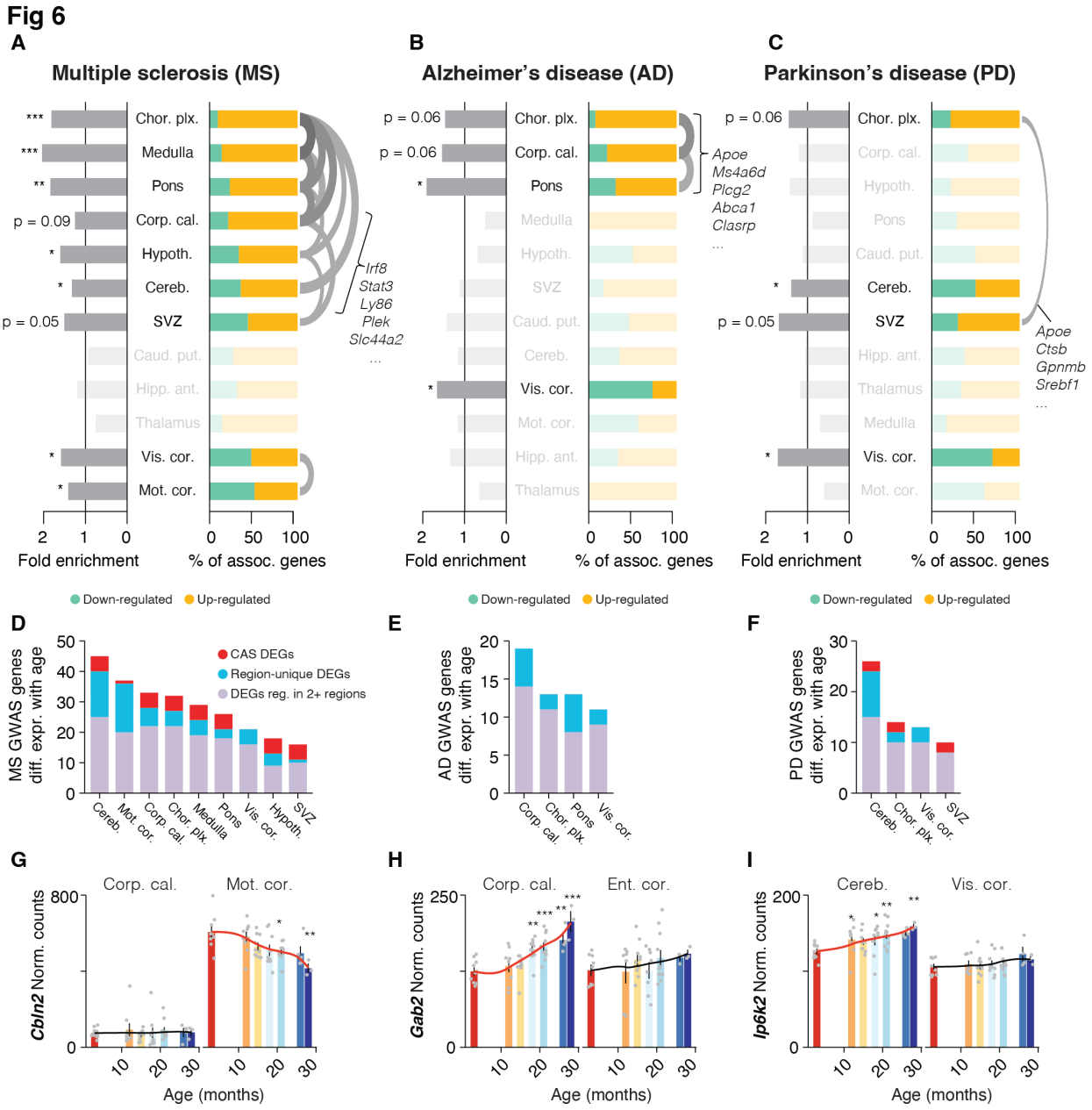

Fig. 6 Interplay of region and age shapes expression of disease variant homologues

(A-C) Enrichment analysis of region-resolved DEGs for human GWAS variants for (A) MS, (B) AD and (C) PD. Associated genes are listed in data S10. Fold enrichment (left bars) and the relative composition of disease-associated DEGs with respect to their regulation (right bars) is indicated. Regions with no significant enrichment are transparent. The vertical order of regions results from hierarchical clustering on a pairwise Jacquard Distance matrix, so regions with overlapping DEGs

will cluster together. Gene overlaps with a Jaccard index ≥ 0.25 are indicated with an arc. One-sided Fisher's exact test with hypergeometric distribution, Benjamini–Hochberg correction. *** $p < 0.001$, ** $p < 0.01$, * $p < 0.05$. (D-F) Number of DEGs per region that are homologues of human GWAS variant for (D) MS, (E) AD and (F) PD. Colors group the genes into CAS DEGs, region-specific DEGs or other (DEG in 2 or more but less than 10 regions). (G-I) Bulk expression in selected regions for (G) *Cbln2*, (H) *Gab2* and (I) *Ip6k2*. Black lines indicate averaged-smoothed gene expression. The trajectory with significant age effect is highlighted. Data are mean ± s.e.m.